JOURNAL OF SCIENCE, TECHNOLOGY AND ENGINEERING RESEARCH
Bilim, Teknoloji ve Mühendislik Araştırmaları Dergisi
ISSN (Online) 2717-8404
Available *online* at https://dergipark.org.tr/en/pub/jster

RESEARCH ARTICLE

Effect of Triangle Fin Inclination Angle and Aluminum Metal Foam on Melting Process in A Vertical Latent Heat Energy Storage System

[*] Emrehan Gürsoy, [1] Mehmet Gürdal, and [2] Engin Gedik

[*]Kardemir Karabük Iron Steel Industry Trade & Co. Inc., Karabük, Türkiye
emrehangursoy@gmail.com, Orcid.0000-0003-2373-3357
[1]Department of Mechanical Engineering, Kastamonu University, Kastamonu, Türkiye
mgurdal@kastamonu.edu.tr, Orcid.0000-xxx-0003-2209-3394
[2]Department of Mechanical Engineering, Kastamonu University, Kastamonu, Türkiye
egedik@karabuk.edu.tr, Orcid.0000-xxx-0002-3407-6121

Citation:
Gursoy, E., Gurdal, M., Gedik, E. (2025) *Effect of Triangle Fin Inclination Angle and Aluminum Metal Foam on Melting Process in A Vertical Latent Heat Energy Storage System*, Journal of Science, Technology and Engineering Research, (6):1, 11-30.DOI: 10.53525/jster.1635055

HIGHLIGHTS

- *Effect of triangles fin structure on melting and energy storage performance has been investigated.*
- *MF significantly changed the natural convection behavior in the LHTES.*
- *87.5 times reduction is realized in the melting time because of MF.*
- *In the analyzed systems, stored energy of 54.83 kJ.m^{-1} is achieved.*

Article Info

Received: February 7, 2025
Accepted: February 19, 2025

DOI: 10.53525/jster.1635055

***Corresponding Author:**
Emrehan Gürsoy
emrehangursoy@gmail.com
Phone: +90 535 687 1526

ABSTRACT

The main objective of this numerical study is to investigate the effect of triangle fin inclination angles (IAs) on the melting process in a Latent Heat Thermal Energy Storage (LHTES) system designed as a vertical rectangular cavity with and without metal foam (MF). In the cases, paraffin wax phase change material (PCM) filled the entire domain, and the Brinkman-Darcy-Forchheimer model, assuming local thermal equilibrium (LTE), and the enthalpy-porosity method were employed to simulate the melting process. In total, 14 different cases were analyzed and the results were validated with literature at high accuracy. Melting time, stored energy, temperature variation, and hydrodynamical behavior of the melting derived from numerical simulations are provided. The findings highlight that utilizing MF has reduced the melting time by 87.5 times and it provided a uniform melting due to enhancing the thermal conductivity of the domains. Also, MF has varied melting behavior and the shortest melting time was realized at 120° without MF, while cases with MF experienced the earliest melting at R-60°. However, using MF decreased the stored energy amount at the rate of 5.69% while the highest energy storage was realized without MF of R-60° as 54.83 kJ.m^{-1}.

Keywords: *Latent heat thermal energy storage; Melting; Metal foam; Phase change material; Triangle fin.*

I. INTRODUCTION

The increasing global temperature and the ongoing climate crisis are widely recognized challenges. In response, 175 nations have committed to the Paris Agreement, aiming to reduce greenhouse gas emissions by 45% by 2030 and achieve net-zero emissions by 2050. Despite these commitments, the International Energy Agency's 2023 report reveals that 80% of global energy consumption is still derived from non-renewable sources, highlighting a significant gap between current efforts and energy demands. To address this disparity, greater emphasis must be placed on the research and development of renewable energy technologies. However, renewable energy sources such as solar and wind are inherently limited by variability in weather, seasonal changes, and time of day. To mitigate these challenges, advanced energy storage systems, including batteries, thermal energy storage (TES), pumped hydro storage, flywheel energy storage, compressed air energy storage, hydrogen energy storage, and supercapacitors, have been developed. Recent advancements in these technologies demonstrate significant progress, suggesting their growing potential to support renewable energy integration.

TES plays a crucial role in balancing the supply and demand of energy, particularly in optimizing intermittent energy sources like solar thermal systems. Among the various TES approaches, LHTES offers a promising alternative to conventional sensible heat storage systems due to its higher energy density potential. LHTES typically utilizes solid-liquid PCMs, which store or release energy at a constant temperature, known as latent heat. These materials are advantageous because of their narrow temperature range, cost-effectiveness, reusability, and ease of integration into thermal systems. Furthermore, they demonstrate significantly higher energy storage densities compared to sensible heat storage fluids such as oil, air, or water. However, one of the key challenges of PCMs is their low thermal conductivity, which significantly impacts system performance [1]. Consequently, various strategies have been developed to enhance their heat transfer capabilities.

Choure et al. [2] categorized techniques to improve the thermal conductivity of PCMs into four main groups: a) the use of high thermal conductivity materials, b) modification of geometry, c) incorporation of multiple phase change materials, and d) the integration of fins with various shapes. Among these, the use of MF, which falls under the first category, is particularly prominent due to its high thermal conductivity, large heat transfer surface area, and low thermal resistance. For instance, Liu et al. [3] explored both experimentally and numerically the effect of non-uniform MF embedded in PCM to mitigate the negative impacts on solar systems and improve solar energy utilization. Their study demonstrated that natural convection accelerated the PCM melting process and inhibited solidification. The optimal conditions for PCM melting and solidification were found to be in the range of $\varepsilon = 0.94$ with specific porosity values for each process. Notably, reductions of 9.7% and 6.2% in the consumption time for melting and solidification processes, respectively, were observed. Liu et al. [4] conducted a study on LHTES using multiple PCMs and MF structures showed significant improvements in thermal performance. The key quantitative findings show that the use of multiple PCMs reduced the complete melting time by 9.18% compared to a single PCM with uniform MF. A one-dimensional positive porosity gradient reduced the melting time by 6.18%, while a negative gradient increased it by 19.78%. On the other hand, the optimal two-dimensional porosity gradient multi-PCM storage system reduced the complete melting time by 17.96% and increased energy storage efficiency by 20.16% compared to the single PCM system with uniform porosity.

The study published by Xing et al. [5] investigated the use of water embedded in copper MF to enhance TES performance, both numerically and experimentally. The effects of the filling ratio, MF specification, and arrangement on heat transfer during the solidification/melting process were analyzed. Results indicated that as the filling ratio increased from 0 to 6.6%, the cold storage/release rate and overall heat transfer coefficient increased, while thermal cycle time, supercooling, and cold storage/release capacity decreased. Notably, heat conduction increased from 67.72% to 91.22% as the filling ratio rose from 3.2% to 6.6%, indicating that heat conduction dominates at higher filling ratios. Yang et al. [6] highlighted significant advancements in LHTES by incorporating graded MFs and active flipping methods to enhance heat transfer and mitigate the low thermal conductivity of PCMs. Key findings reveal that optimal thermal performance occurs at a 6% porosity gradient and a dimensionless flipping time of 0.4, reducing melting time by 49.37% and improving the thermal energy storage rate by 76.23%. Shen et al. [7] employed a solid-

liquid lattice Boltzmann model at the REV scale to examine how gradient porosity enhances LHTES. Among three gradient porosity configurations-Chinese-fan-shape, vertical, and concentric-the fan-shape arrangement delivers the best performance, reducing melting time by 36.1% compared to homogeneous porosity while achieving better temperature uniformity. Increasing the number of layers beyond two yields minimal improvements in melting time (up to 4.4%), whereas higher porosity gradients significantly increase melting time by at least 36.1%. Alasmari et al. [8] investigated the role of a 30% MF layer in enhancing heat transfer in LHTES systems on both the heat transfer fluid side and the shell side. Using a two-temperature heat equation model and finite element analysis, the research reveals that optimizing the MF layer's position and shape parameter (FL) can significantly reduce melting time by approximately 40%. At an inlet pressure of 750 Pa, increasing the FL parameter from 0.75 to 1.37 raises energy storage power during 90% charging from 32.2 W to 48.7 W, marking a 34% improvement. These findings highlight the potential of MF integration for improved thermal performance in LHTES systems. Bouzidi et al. [9] explored the application of anisotropic MF with tailored local characteristics to enhance heat transfer in LHTES. Unlike previous research on partial MF, this work integrates heterogeneous copper foam into a shell-tube system with paraffin wax, analyzing various heterogeneity angles (-90° to 90° in 15° increments) using finite element methods. Results reveal that the most effective configuration, with a 0° heterogeneity angle, reduces charging and discharging times to 623 and 989 minutes, respectively, compared to 646 and 1007 minutes for uniform MF.

Ahmed et al. [10] experimentally evaluated the heat storage properties of PCMs enhanced with copper and iron-nickel MFs. The thermal behavior of paraffin within these composites is compared to pure paraffin under a constant heat flux of 1000 $W.m^{-2}$ across three directions. Results show that incorporating MFs significantly improves thermal conductivity, with copper MF/paraffin composites achieving superior temperature uniformity compared to iron-nickel MF/paraffin composites and pure paraffin. Notably, the copper MF/paraffin composite reduces heat storage time to 20.63% of the time required by the iron-nickel MF/paraffin composite, highlighting its efficiency in enhancing thermal performance. Nassar et al. [11] aimed to enhance the low thermal conductivity of conventional PCMs by investigating composites with MFs and hybrid nanoparticles. Results indicate that increasing the weight percentage of MF and nanoparticles improves thermal conductivity, achieving a 37.7% enhancement for copper-based composites. The optimal specific surface value of 1600 $m^2.m^{-3}$ delivers superior thermal performance. While increased MF content also enhances heat capacity, the fixed shapes of MFs pose challenges in compatibility with PCM formability, limiting their use in compact applications. Liu et al. [12] conducted a pore-scale numerical analysis of PCM melting in a truncated cuboctahedron (TCD) and tetrakaidecahedron (TKD) MF. Results reveal that natural convection reduces melting time by about 7% within the examined porosity range. The TCD MF accelerates melting in the early stage due to its larger surface area, while the TKD MF is more effective in the later stage due to thicker metallic ligaments. A critical porosity threshold determines which structure provides superior enhancement, shifting from TCD to TKD as porosity decreases. At porosity of ε=0.941, both foams yield similar total melting times, but half-melting occurs faster in TCD (17.2%) compared to TKD (20.3%), highlighting structural influence on phase transition dynamics.

Du et al. [13] investigates the enhanced heat transfer properties of MF in a LHTES system. A 3D transient numerical model of a horizontal square cavity LHTES unit is developed to analyze the impact of MF on melting and solidification processes. An experimental LHTES system is constructed for model validation. The Taguchi method is used to evaluate the effects of MF porosity (ε) and pore density (ω) on phase transformation, heat charging, and discharging times. Results indicate that MF porosity has a greater impact on the phase transformation process than pore density. For example, the melting-solidification time of Case 3 (ε=0.97, ω=30 PPI) is 67.46% shorter than that of Case 9 (ε=0.99, ω=30 PPI). Additionally, Case 3 shows a 199.33% increase in heat charging efficiency and a 196.35% improvement in heat release efficiency compared to Case 9.

The number of studies investigating the effect of fin types on LHTES performance shows an increment in the last years. Within this scope, Moaveni et al. [14] conducted a study on the thermal management of lithium-ion batteries under maximum performance and safety conditions. Their findings showed that adding nanoparticles (φ =

9.0%) and using four fins reduced the peak temperature by 5.18K and 10.36K at a 4C discharge rate, respectively. Additionally, the application of copper MF (ε=0.90) reduced the temperature by 12.57K at a 3C discharge rate. The study carried out by Yang et al. [15] on LHTES using solid-liquid PCM found that the optimal configuration of finned MF with graded porosity significantly improves thermal performance. Specifically, compared to the base case, this configuration shortens melting time by 46.68%, increases the TES rate by 74.06%, and increases the Nusselt number by 69.02%. Besides, the optimal parameters have been acquired as a fin length of 20 mm, a fin width of 1.5 mm, a porosity gradient of 2%, and a rotational speed of 0.5 rpm. A novel staggered fin-foam design is proposed by Lu et al. [16] to assess the impact on melting performance in shell-and-tube. The straight fin-foam configuration reduces melting time by 58.67% compared to foam-only designs. Further improvements are seen with a segmented staggered configuration, with the optimal design (four segments) reducing melting time by an additional 13.18%. This configuration enhances heat transfer and lowers the outlet temperature by 23.55 K, improving heat utilization. Rahmanian et al. [17] examined the various LHTES systems with different MF fin configurations that were simulated and compared to pure PCM and fully MF enclosures. Two boundary conditions, constant temperature, and constant heat flux, were considered. Results showed that MF fins significantly improved thermal performance under constant temperature conditions. For systems with six MF fins, melting times were reduced by 42% and 30% under constant temperature and heat flux conditions, respectively. Additionally, the input heat rate was enhanced by up to 112% and 155% for systems with 6 MF fins and fully MF configurations, respectively.

Hasan et al. [18] investigated the impact of two fin configurations, I-shaped and V-shaped, on the solidification process of a paraffin-based PCM loaded with CuO nanoparticles. The configurations were designed to maintain the same volume of paraffin. Numerical simulations using the Finite Volume Method (FVM) and an implicit technique revealed that the system with I-shaped fins required 8.93% less time for solidification than the V-shaped fins. The freezing times were 47.26 minutes for the I-shaped fins and 51.89 minutes for the V-shaped fins, indicating that the I-shaped fins enhanced solidification performance. Zhang et al. [19] studied the heat transfer mechanisms in shell-and-tube and annular finned shell-and-tube latent TES systems. They discovered that both convection and heat conduction are key to the heat transfer process in the annular finned shell-and-tube TES. However, natural convection led to uneven melting, affecting liquid fraction and temperature uniformity. To better utilize natural convection during the melting process, several innovative annular fin configurations have been proposed in the literature. Abhinand S et al. [20] explored the melting behavior in a LHTES using ice as the PCM and fins to enhance thermal performance. The research aims to determine the optimal number of fins to improve heat transfer and minimize melting time in the tube. Various parameters, such as tube arrangement, diameter, and temperature, were evaluated for their impact on charging performance. The findings show that increasing the number of fins from 4 to 15 boosts the generated liquid PCM by 34.69%, with a subsequent decrease of 9.03% beyond 15 fins. A staggered tube arrangement improves melting performance compared to an inline arrangement. Additionally, a higher tube temperature (280 K) produced 2.08 times more liquid PCM than at 275 K, and increasing the tube diameter from 5 mm to 20 mm enhanced the charging process, generating 2.68 times more liquid PCM.

Fahad et al. [21] investigated the impact of six modified longitudinal fin designs in a shell-and-tube heat exchanger unit on the charging and discharging of PCM. The designs include modifications to the traditional rectangular fin shape (Case 1), with variations such as tapering (Case 2), inverse tapering (Case 3), herringbone wavy (Case 4), convex (Case 5), and constricted (Case 6) shapes. The performance of the designs was assessed based on the total phase transition time, melting time, and solidification time. Case 4, with the herringbone wavy shape, showed the best performance, improving total phase transition time by 10.93%, melting time by 8.48%, and solidification time by 12.31% compared to the traditional rectangular fin. Conversely, Case 5, the convex shape, performed the worst, with decreases of 3.55%, 5.88%, and 5.04% in total cycle time, melting time, and solidification time, respectively, compared to the base case. Farahani et al. [22] examined the numerical analysis of heat transfer and PCM melting enhancement in a three-dimensional cylindrical LHTES system using RT82 as the PCM. The study investigates the effects of strip fins, Fe_3O_4 nanoparticles, and both uniform and non-uniform magnetic fields on PCM melting. The results show that the introduction of strip fins reduces the PCM melting time by approximately 51%

compared to no fins. Abdulrazzaq et al. [22] focused on improving the performance of PCM-based shell-and-tube LHTES systems by utilizing differently shaped fins. PCM systems face challenges due to their low thermal conductivity, which this study addresses by incorporating conductive fins. The system consists of concentric cylinders, where the inner cylinder carries the heat transfer fluid and the outer one contains the PCM. Four different fin shapes (straight, curved, and wavy) are attached to the heat transfer fluid cylinder. The results indicate that the use of a curved fin reduces the melting time by 122.2% compared to the no-fin case. The findings demonstrate that modifying the geometry of the system significantly enhances the heat energy storage rate, offering valuable insights for designing more efficient and compact thermal energy storage systems. Ao et al. [23] explored the enhancement of heat transfer efficiency in LHTES units using novel three-tube heat exchangers with longitudinal fins. The research investigates the impact of fin number, length, thickness, and arrangement on the melting performance of PCM. The results show that thinner and longer fins significantly reduce the melting time, with the complete melting time of thin long fins being 10.6% faster than short thick fins. The optimal fin length was found to be 30 mm, which shortened the heat storage time by 18%. Additionally, a lower long and upper short fin arrangement improved heat transfer efficiency. Du et al. [24] compared the heat storage and release performances of four structures: pure paraffin, fins, MF, and fin-MF, throughout the complete melting-solidification cycle. Using experimental snapshots and real-time data acquisition, the study evaluates phase interface changes and internal temperature variations. Results show that both fins and MF improve melting and solidification, with fins offering better temperature responses and MF providing greater temperature uniformity. The combination of fins and MF demonstrates the best heat storage/release performance, reducing heat storage and release time by 61.6% and 82%, respectively, and improving average temperature response by 122.4% and 429.8% compared to pure PCM.

Huang et al. [25] used numerical analysis to investigate heat storage and release in a square LHTES unit, enhanced by fins, MF, and a periodic sinusoidal heat source. An experimental setup validates the numerical findings, and the Box-Behnken design in response surface methodology is used for optimization. The results show that fin position and MF pore density do not impact the PCM volume. The initial design with evenly spaced fins creates a refractory zone during phase transformation, with temperature fluctuations due to heat source instability. Optimal results indicate that increasing transverse fin spacing reduces total storage-release time, while increasing longitudinal fin spacing and pore density initially decreases and then increases storage-release time. The optimal structure achieved a 29.55% reduction in total storage-release time, a 20.74% increase in average heat storage rate, and a 65.75% increase in heat release rate during solidification compared to Case 1.

Zeng et al. [26] introduced a novel fin-MF combination to enhance melting and solidification in horizontal shell-and-tube latent heat storage devices. Upward fins accelerate natural convection, while downward foams improve thermal conduction. Numerical analysis compares this design with typical eccentric and concentric configurations throughout the full phase change cycle. The fin-MF combination achieves the best performance, reducing melting time by 47.9% and solidifying time by 55.4%, while minimizing the "buckets effect" in eccentric designs by lowering the melting-solidifying time difference to 12%. The existing literature indicates that numerous studies have explored the heat transfer characteristics of LHTES systems enhanced by MF under various conditions, including natural convection. However, further investigation is needed regarding the specific impact of triangular fin structures and their varying IAs in the context of PCM-MF hybrid systems. Such systems have potential applications in a wide range of fields, including solar energy systems [27], microelectronics [28], and building thermal management [29].

Building on this gap in the literature, the present study examines in detail the heat transfer, heat storage, and melting performance of triangular-finned rectangular cavities filled with PCM and embedded with MF. A numerical study has been conducted to explore the effects of triangular fin IAs, along with the presence of tending and aluminum-based MF, under laminar flow and natural convection conditions.

II. MODEL DESCRIPTION

A two-dimensional schematic representation of the computational domain is illustrated in Figure 1. The domain consists of a rectangular cavity with dimensions of 30 mm in height (H) and 10 mm in width (W). It is filled alternately with pure PCM and PCM combined with MF to compare cases with and without MF structure. The left wall of the domain is maintained at a constant temperature of 335.15 K, while the remaining walls are treated as adiabatic with no-slip conditions. The initial temperature across the domain is set at 298.15 K. The top wall features a triangular geometry, with IAs varying along its length from left to right. This study aims to analyze heat transfer behavior within the PCM during the melting process when encountering obstacles. Rubitherm RT58 paraffin wax, an organic PCM, was selected for the study. The MF, assumed to be aluminum, was characterized by a porosity of ε=0.9 and a pore density of ω=20 PPI.

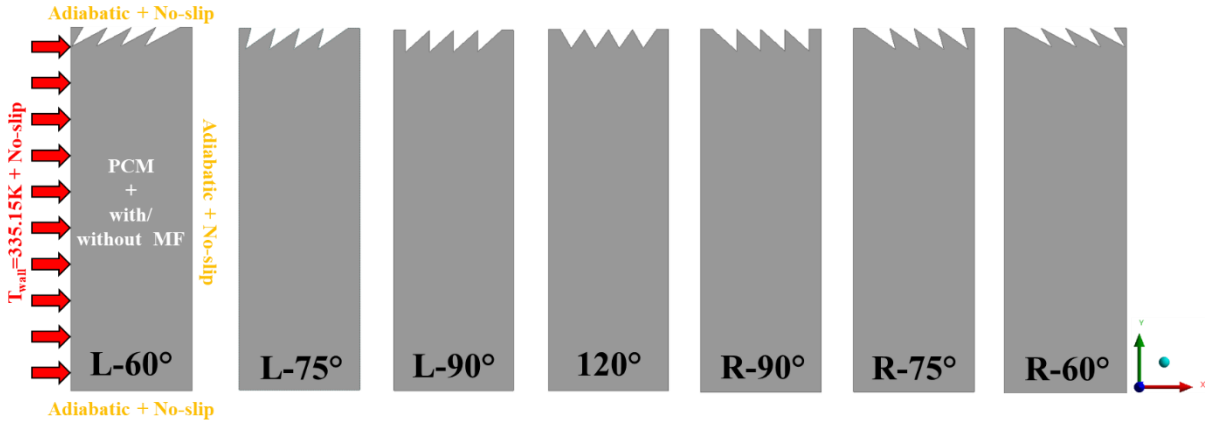

Figure 1. Schematic view and boundary conditions of the computational domain.

The Forchheimer-extended Darcy model has been utilized to simulate heat transfer between the PCM and MF, incorporating the LTE hypothesis. This hypothesis assumes that the time-averaged internal temperatures of the fluid and solid phases are equal, with supporting studies in the literature validating its applicability for aluminum MF with a ω=20 PPI [30], [31]. The study operates under the following assumptions:

i. The liquid phase of the PCM behaves as a Newtonian and incompressible fluid.
ii. Except for density, the thermophysical properties of both the PCM and MF remain constant regardless of the phase change.
iii. The Boussinesq approximation is applied to account for density variations due to buoyancy effects in the momentum equation, given the small temperature differences.
iv. The MF is considered homogeneous and isotropic in all directions.
v. The domain volume is assumed to remain constant throughout the melting process.

The governing equations for the PCM and MF combination are provided below, derived from the stated assumptions and hypotheses. The enthalpy-porosity method is employed to model the melting process.

This approach does not explicitly track the melt interface; instead, it assigns a liquid fraction to each cell within the computational domain. This fraction quantifies the proportion of the cell volume that exists in the liquid state and is determined iteratively using an enthalpy balance [32]. Based on this methodology, the continuity equation is expressed as shown in Eq. (1) [33].

$$\nabla \cdot V = 0 \tag{1}$$

where V denotes the velocity field within the computational domain. The momentum equation, which governs the fluid motion, is provided in Eq. (2) [34].

$$\frac{\rho_p}{\varepsilon}\frac{\partial V}{\partial t}+\frac{\rho_p}{\varepsilon^2}V\cdot\nabla V = -\nabla P+\frac{\mu_p}{\varepsilon}\nabla^2 V-\frac{(1-\beta)^2}{(\beta^3+0.001)}A_{mush}V-\left(\frac{\mu_p}{K}V+\frac{C_F}{\sqrt{K}}\rho_p V|V|\right)+\rho_p g\gamma\Delta T_0 \quad (2)$$

in which ρ_p [kg.m^{-3}], μ_p [Pa.s], and γ [K^{-1}] describe the density, dynamic viscosity, and thermal expansion coefficient of PCM, respectively. Furthermore, ε, β, A_{mush} [kg.m^{-3}.s^{-1}], C_F [m^{-1}], g [m.s^{-2}], ΔT_0 [K], K [m^2], and P [Pa] show the porosity of MF, liquid fraction, mushy constant (set to 10^5 kg.m^{-3}.s^{-1}),

Forchheimer drag (inertial) coefficient, gravity (set to 9.81 m.s^{-2}), the temperature difference relies on the Boussinesq approximation, permeability, and pressure. The energy equation written in Eq. (3) is considered due to the LTE hypothesis [33].

$$(\rho c)_{eff}\left(\frac{\partial T}{\partial t}+V\cdot\nabla T\right)=k_{eff}\nabla^2 T-\varepsilon\rho_p H_L\frac{\partial\beta}{\partial t} \quad (3)$$

The term k_{eff} [W.m^{-1}.K^{-1}], as defined in Eq. (4), represents the volume-averaged effective thermal conductivity within the fluid and MF region, while H_L [J.kg^{-1}] denotes the latent heat of the PCM [32].

$$k_{eff}=\varepsilon k_{PCM}+(1-\varepsilon)k_{MF} \quad (4)$$

The terms in the momentum equation related to MF need to be defined using validated mathematical expressions. To achieve this, the permeability of the MF is determined using Eq. (5) [35].

$$K=\frac{\varepsilon^2 d_k^2}{36\,(\delta^2-\delta)} \quad (5)$$

The parameters d_k [m] and δ represent the characteristic length and the tortuosity coefficient of the MF, respectively. These parameters are defined using Eqs. (6) and (7) [35].

$$d_k=\frac{\delta}{3-\delta}d_p \quad (6)$$

$$\delta=2+2\cos\left[\frac{4\pi}{3}+\frac{1}{3}\cos^{-1}(2\varepsilon-1)\right] \quad (7)$$

The Forchheimer's drag (inertial) coefficient is determined using Eq. (8) [35].

$$C_F=0.00212(1-\varepsilon)^{-0.132}\left(\frac{d_f}{d_p}\right)^{-1.63} \quad (8)$$

The parameters d_f [m] and d_p [m] represent the fiber diameter and pore diameter of the MF, respectively, and can be calculated using Eqs. (9) and (10) [35].

$$d_f = 1.18\sqrt{\frac{1-\varepsilon}{3\pi}}\left(\frac{1}{1-e^{\left(-\frac{1-\varepsilon}{0.04}\right)}}\right) \tag{9}$$

$$d_p = \frac{0.0254}{\omega} \tag{10}$$

The pore density, ω [PPI], is specified as 20 PPI. In solidification and melting phenomena, one of the critical parameters is the liquid fraction (β). This parameter, incorporated into the momentum equation (Eq. (2)), varies within the range $0 \leq \beta \leq 1$ based on the solidus and liquidus temperatures. Consequently, the equation describing the variation of β is provided in Eq. (11) [35].

$$\beta = \frac{\Delta H}{H_L} = \begin{cases} 0 \; if \; T < T_S \\ \dfrac{T - T_S}{T_L - T_S} \quad if \; T_S < T < T_L \\ 1 \; if \; T > T_L \end{cases} \tag{11}$$

T_S [K], T_L [K], and T [K] represent the solid phase temperature, liquid phase temperature, and local temperature, respectively. Additionally, β depends on the local temperature (T), with PCM starting to melt when T exceeds T_S. The variation in enthalpy, which reflects the stored energy, can be determined using Eqs. (12)-(14) [33].

$$\Delta H = \Delta H_{PCM} + \Delta H_{MF} = \varepsilon \int (\rho \Delta h)_{PCM} dA + (1-\varepsilon) \int (\rho \Delta h)_{MF} \, dA \tag{12}$$

$$(\rho \Delta h)_{MF} = c_{p_{MF}}(T_{MF} - T_{in}) \tag{13}$$

$$(\rho \Delta h)_{PCM} = \begin{cases} c_{p_{PCM,S}}(T_{PCM} - T_{in}) \; if \;\; T_{PCM} < T_S \\ c_{p_{PCM,S}}(T_s - T_{in}) + H_L \beta \; if \;\; T_S < T_{PCM} < T_L \\ c_{p_{PCM,S}}(T_S - T_{in}) + H_L + c_{p_{PCM,L}}(T_{PCM} - T_L) \; if \; T_L < T_{PCM} \end{cases} \tag{14}$$

in which ΔH_{PCM} and ΔH_{MF} represent the enthalpy variations of the PCM and the MF, respectively, while their sum constitutes the total enthalpy variation (ΔH) of the TES system. Additionally, h, A, and T_{in} denote the specific enthalpy, volume, and initial temperature of the TES system, respectively. In the analyses, RT58 (Rubitherm) has been used as the PCM, and aluminum MF has been selected for the study. The thermophysical properties of these materials are listed in Table 1.

Table 1. Thermophysical properties of RT58 PCM and aluminum MF [33].

Properties	RT58	Aluminum
Density, ρ [kg.m^{-3}]	825	2719
Specific heat, c_p [J.kg^{-1}.K^{-1}]	2000	871
Thermal conductivity, k [W.m^{-1}.K^{-1}]	0.2	202.4
Dynamic viscosity, μ [kg.m^{-1}.s^{-1}]	0.0269	-

Thermal exp. coeff., γ [K^{-1}]	0.00011	-
Latent heat, H_L [$J.kg^{-1}$]	160000	-
Solidus temperature, T_s [K]	326	-
Liquidus temperature, T_L [K]	332	-

Following the critical information outlining the problem under investigation, the solution methodology for the numerical analysis is defined. The analyses were performed using ANSYS Fluent 2024 R1 software, which employs the FVM for calculations. The pressure-velocity coupling was resolved using the SIMPLE algorithm and its prefer to increase the robustness and efficiency handling incompressible flow and strong coupling between temperature, velocity, and pressure fields [36]–[38]. The SIMPLE algorithm ensures proper pressure-velocity coupling by iteratively correcting velocity fields, which is essential for conserving mass in phase change processes [39]. It effectively handles low-speed buoyancy-driven flows, stabilizing the pressure and velocity fields in transient melting/solidification problems [40]. Pressure was calculated with the PRESTO algorithm because its superior accuracy in handling pressure gradients in the case with strong body force including natural convection-driven phase change [41]. The PRESTO! scheme enhances pressure interpolation, reducing numerical artifacts like checkerboarding and improving pressure gradient resolution. Since phase change is often accompanied by natural convection, PRESTO! provides higher accuracy in buoyancy-driven flows by refining the pressure field distribution [42].

By combining SIMPLE and PRESTO!, software achieves greater numerical stability and physical realism in melting process, ensuring reliable predictions of phase change dynamics. Besides, under-relaxation factors were set as 0.3 for pressure, 1.0 for density, 0.7 for momentum, 0.9 for liquid fraction, and 1.0 for energy. Additionally, the convergence criteria were established as 1×10^{-6}, 1×10^{-5}, and 1×10^{-6} for continuity, momentum, and energy, respectively.

To evaluate the effects of mesh density and time step size, convergence and sensitivity analyses were performed for the case of 120° including MF. The fluid domain was discretized into small volume cells using local mesh settings, independent of mesh quality metrics. A mesh convergence analysis was conducted for three different mesh densities. The quality metrics, specifically the minimum orthogonal quality, and maximum skewness, were maintained approximately constant at 0.730 and 0.528, respectively.

As illustrated in Figure 2(a), the liquid fraction remains unaffected by varying mesh densities, with a maximum error rate of 0.2% observed compared to the 19400-mesh number. These results indicate that the mesh density does not significantly influence the results. Consequently, the mesh configuration with the 7500-mesh number was selected for further analysis, and its schematic structure is shown in Figure 3. Additionally, a time step sensitivity analysis was performed for t=0.1, 0.5, and 1.0s using the 7500-mesh number configuration. According to Figure 2(b), the trends in the liquid fraction are consistent across all time steps. The maximum error rates in liquid fraction between t=0.1s and t=0.5s, as well as t=0.1s and t=1.0s, were 3.23% and 7.08%, respectively. Based on these findings, t=0.5s was selected as the optimal time step for subsequent analyses.

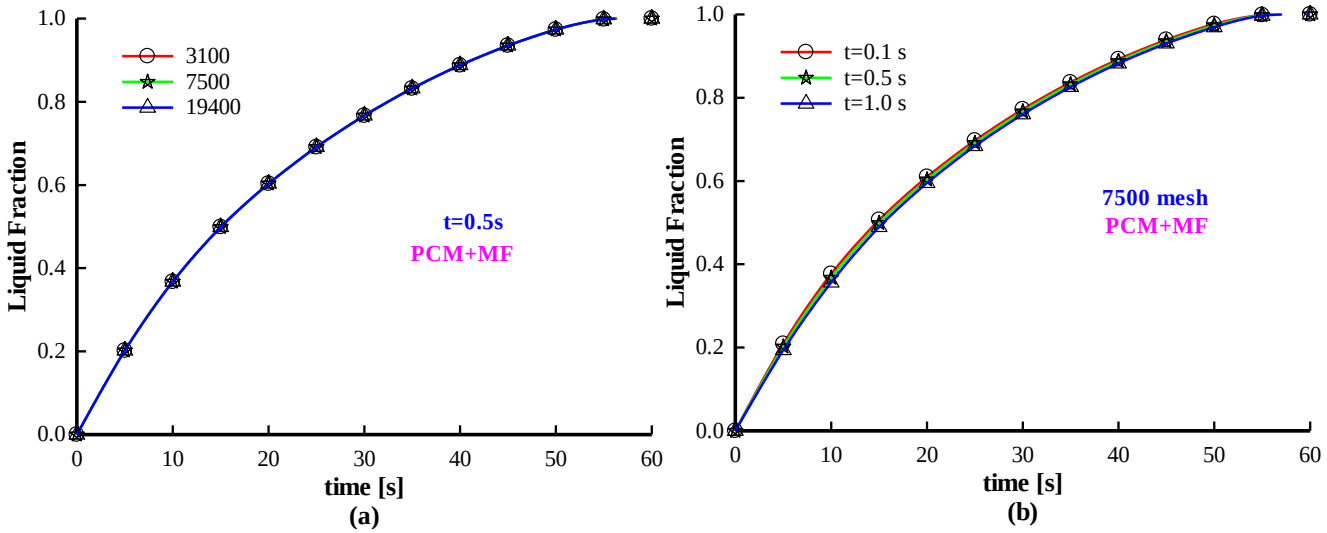

Figure 2. Variation of liquid fraction for; (a) mesh convergence analysis at t=0.5s and (b) time step sensitivity analysis for 7500 mesh number.

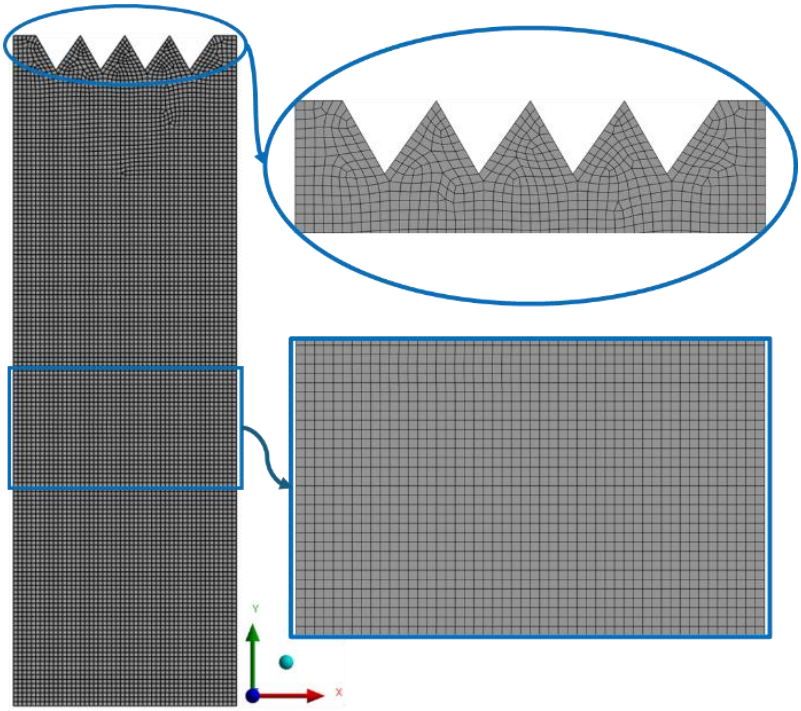

Figure 3. Presenting of the mesh structure with 7500 mesh numbers.

To validate the accuracy of the methods and solutions applied in the numerical study, a validation analysis was performed using data from the literature. The comparative analysis was based on the work of Huang et al. [35] focusing on the liquid fraction in a fluid domain without a fin structure. In order to perform the validation, an exact copy of the study conducted by Huang et al. was designed. The suitability of the mesh study and the selected solution methods was tested in this way. To obtain a complete replica solution data, a vertical rectangular cavity without triangular fins was created and heated with 335.15K from one wall. The other walls were assumed to be adiabatic and no-slip condition was assumed on all walls. A copper MF with porosity and pore density of ε=0.90 and ω=10 PPI, respectively, was placed inside the rectangular cavity and the entire volume was filled with RT42 PCM. The results of the current study were compared with the reference data, as shown in Table 2 and Figure 4, respectively, considering the liquid fraction.

The comparison revealed that the contours demonstrated a high degree of similarity, confirming the reliability of the numerical approach. Besides, liquid fraction trends show a high harmony between each other, and the average deviation has been acquired as 0.83%.

Table 2. Validation of the numerical solution methods via liquid fraction contours as a function of time.

Time, t [s]	60	180	360	540	720	900
Huang et al. [35]						
Present study						

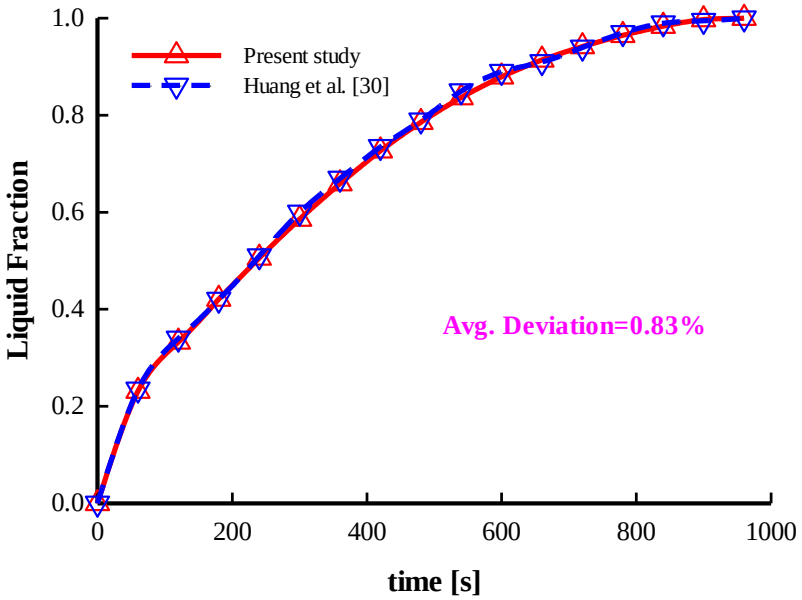

Figure 4. Validation of the numerical solution methods via liquid fraction trends as a function of time.

III. RESULTS AND DISCUSSIONS

The changing of liquid fraction as a function of time is presented in Figure 5 for PCM and PCM+MF cases. Presenting liquid fraction results is critical to understanding heat transfer processes and system performance. A logarithmic growth is seen both each case with increasing time. As the figures examined, LHTES of 120° first reached the full liquid phase on condition including only PCM. Initially, entire cases performed similar melting characteristics. However, 120° provided a considerable difference between the time of t=437.5-2625s compared to other cases, and the difference in melting rate reached up to 15.0% in this period. On the other hand, utilizing MF has accelerated the melting due to increasing the effective thermal conductivity. Also, MF has changed the melting characteristics and the R-60° configuration provided the full liquid phase condition, primarily. The reason for this situation can be attributed to the homogenous behavior of the MF.

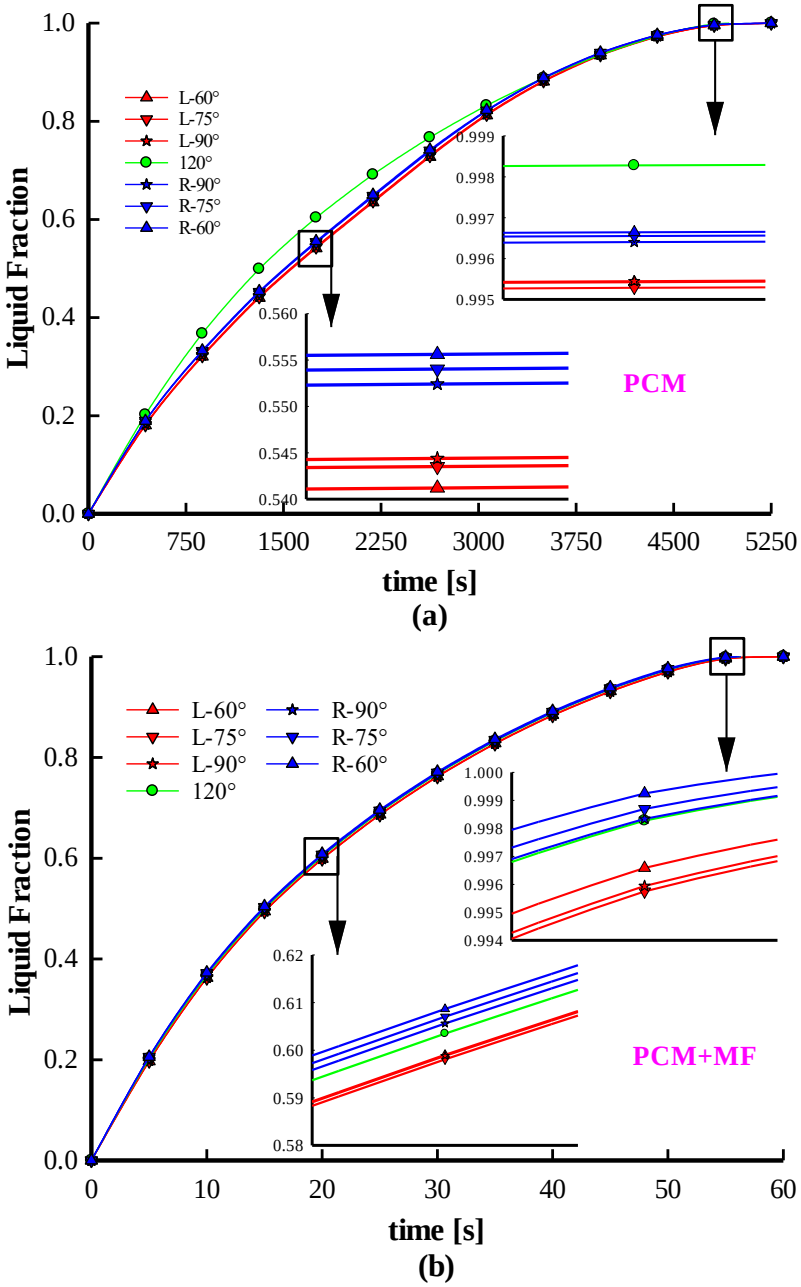

Figure 5. Liquid fraction versus time considering different IAs for; (a) without MF and (b) with MF.

The melting behavior of the LHTES with 120° and R-60° has been visually presented in Table 3. It was concluded that the presence of MF significantly influenced the system's behavior. Specifically, in the absence of MF, the 120° configuration exhibited the highest melting performance. Conversely, in the presence of MF, the R-60° configuration achieved the highest melting performance. Additionally, the liquid fraction of the PCM embedded within MF was found to be more uniformly distributed compared to the PCM without MF. In the case of without MF, natural convection is more dominant than heat conduction. At t=875s, heat mostly progresses with the help of conduction. However, the effect of buoyancy force increased melting behavior progressively and the melted PCM on the bottom side of the rectangular cavity carried out the upper side. Because of this, a natural convection can be observed after the t=875s, and a logarithmic solid-liquid interface is seen at the upper side. In the case of including MF, there is no logarithmic solid-liquid interface and the melting progressed linearly from the left side to the right side because heat conduction is more dominant than natural convection.

Table 3. Comparison of liquid fraction contours belonging to 120° and R-60° LHTES configurations.

Without MF				
Time, t [s]	**875**	**2187.5**	**3500**	**4812.5**
120°	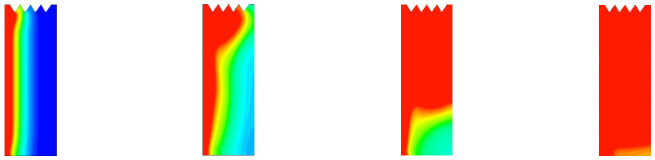			
R-60°	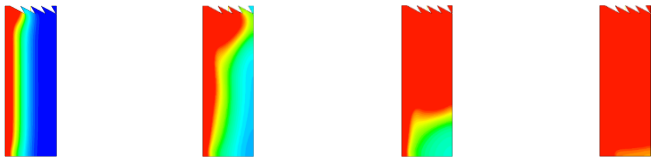			
With MF				
Time, t [s]	**10**	**25**	**40**	**55**
120°	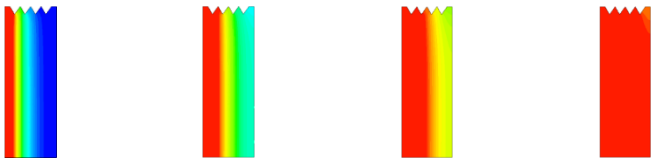			
R-60°				

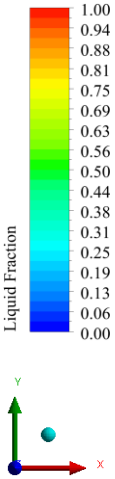

Figure 6 illustrates the influence of MF and the IA of triangular fins on the melting process. Considering the melting time provides important insights in terms of evaluating the thermal response time of the system and determining the heat transfer efficiency. The results indicate that the inclusion of MF significantly reduced the melting time by approximately 87.5 times. This reduction can be attributed to the enhanced effective thermal conductivity of the system, which facilitates better heat conduction and increases thermal diffusion within the domain. Furthermore, MF was found to alter the system's characteristics. As shown in Figure 6(a), the shortest melting time in the absence of MF was observed for the 120° configuration.

However, with the addition of MF, this behavior shifted, and the R-60° configuration achieved the fastest melting time, as depicted in Figure 6(b). The reason for this difference, as mentioned before, is that MF exhibits homogeneous behavior due to heat being transferred via conduction. The accelerated melting of PCM in the presence of MF can be explained by the significant improvement in effective thermal conductivity. This enhancement, combined with the synergistic effects of heat conduction and heat convection, resulted in a faster melting rate of the PCM when MF was included in the system.

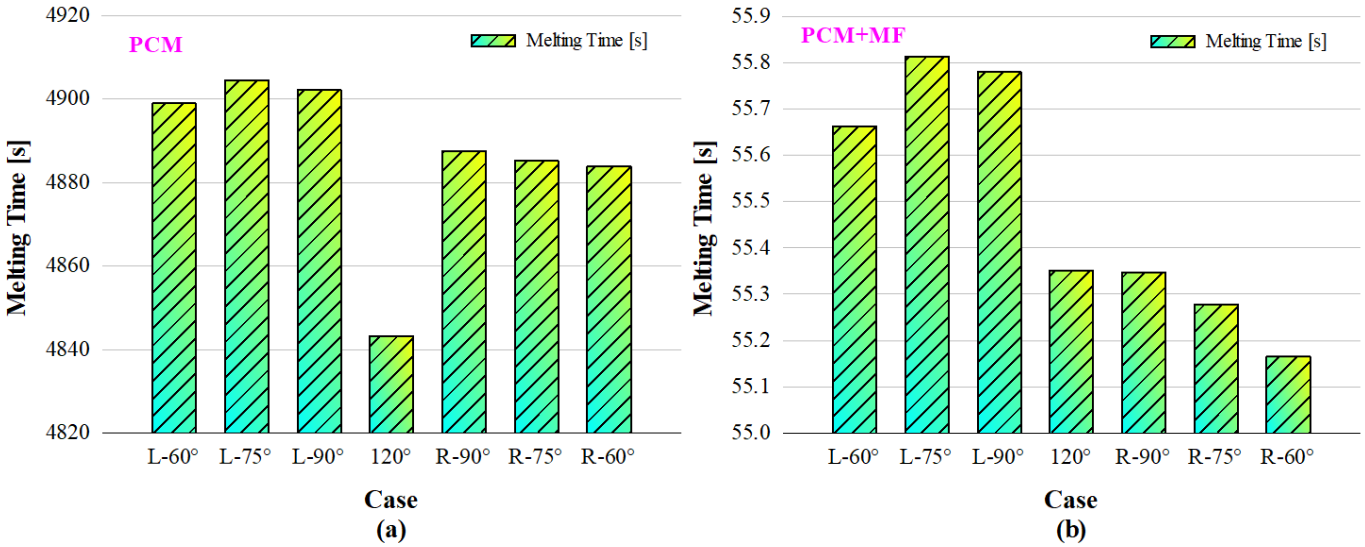

Figure 6. Comparison of melting time considering different IAs for; (a) without MF and (b) with MF.

Figure 7 depicts the temporal average temperature variation in the LHTES systems including different triangle fin configurations. In these applications, evaluating PCM temperature change is crucial for defining the system's phase change process and understanding the heat transfer dynamics. It is clearly mentioned that temperature changes show a sudden increase in the early stage of melting (pre-sensible) for both without MF and with MF cases due in that time heat dominantly progresses with conduction. After the starting of the melting, the latent heat process is observed and temperature variations show a more horizontal tendency.

The results, also, indicate that the highest final temperature was achieved in the R-60° configuration for both cases. The final temperature was recorded as 334.91K without MF and 334.75K with MF.

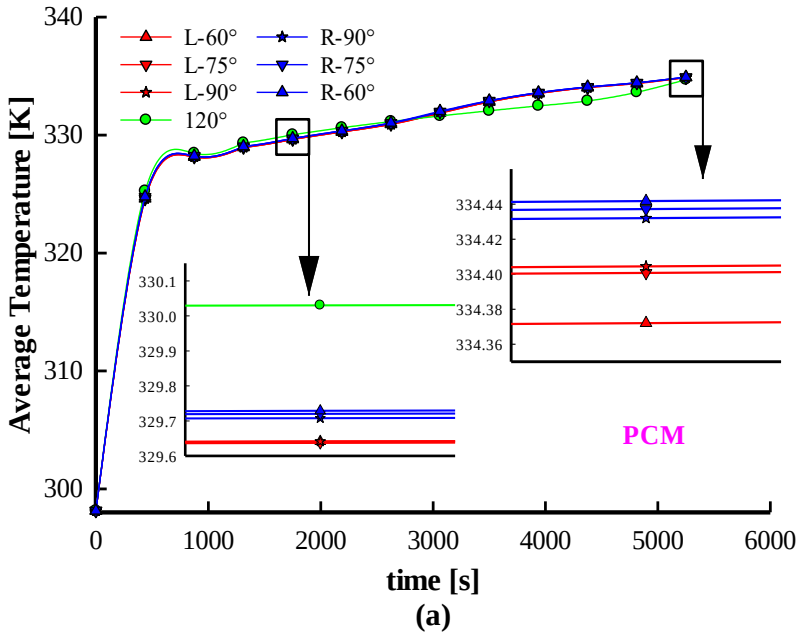

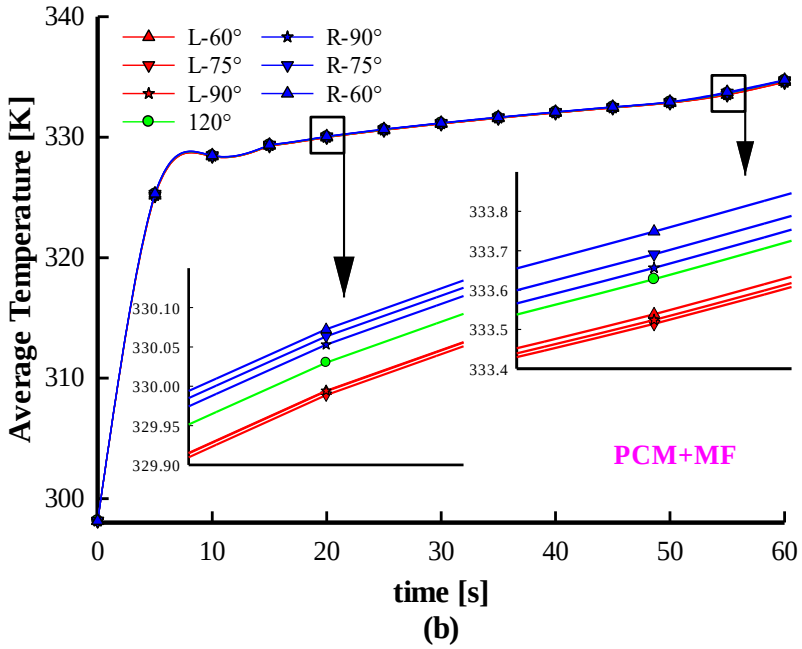

Figure 7. Average temperature versus time considering different IAs for; (a) without MF and (b) with MF.

The velocity profiles of the cases with different triangular IAs, without and with MF, on the horizontal (0, 15 mm; 10 mm, 15 mm) and vertical (5 mm, 0; 5 mm, 30 mm) lines are presented in Figure 8 for fully melted condition. In these applications, discussion of the speed changes in the system is an important indicator of heat transfer effectiveness and understanding the phase change process. When examining the horizontal velocity profiles, it is evident that the MF exerts a significant influence on the velocity distribution within the rectangular cavity. The velocity is observed to be highest in regions adjacent to the lateral walls, with elevated velocity values near the heated wall. This phenomenon is attributed to the thermal gradient established by the heated wall, which induces density variations in the PCM due to thermal expansion. The less dense, heated material ascends along the heated wall, while the denser, cooler material descends along the opposing walls, generating natural convection currents. These convective flows are most pronounced near the walls, where the thermal gradients are steepest, resulting in higher velocities in these regions. Conversely, the velocity values in the central region of the cavity consistently decrease under all conditions. The central region behaves as a "stagnation zone" where the interaction of upward and downward convective currents from opposing walls reduces the net velocity. Notably, under without MF conditions, the lowest velocity profiles occur in the L-60° configuration, whereas under MF influence, the R-60° configuration yields the highest velocity levels.

The effect of MF is also distinctly observable in the vertical velocity profiles. In without MF scenarios, velocity increases near the bottom of the cavity, whereas MF presence leads to a more uniform velocity distribution. Under MF conditions, regions of heightened velocity are shifted toward the upper wall, coinciding with the locations of fins. Furthermore, while the L-60° configuration exhibits the lowest velocity without MF cases, L-90° demonstrates the highest velocity distribution under MF conditions. These findings underscore the critical role of MF in modulating flow dynamics and enhancing velocity distribution within the cavity.

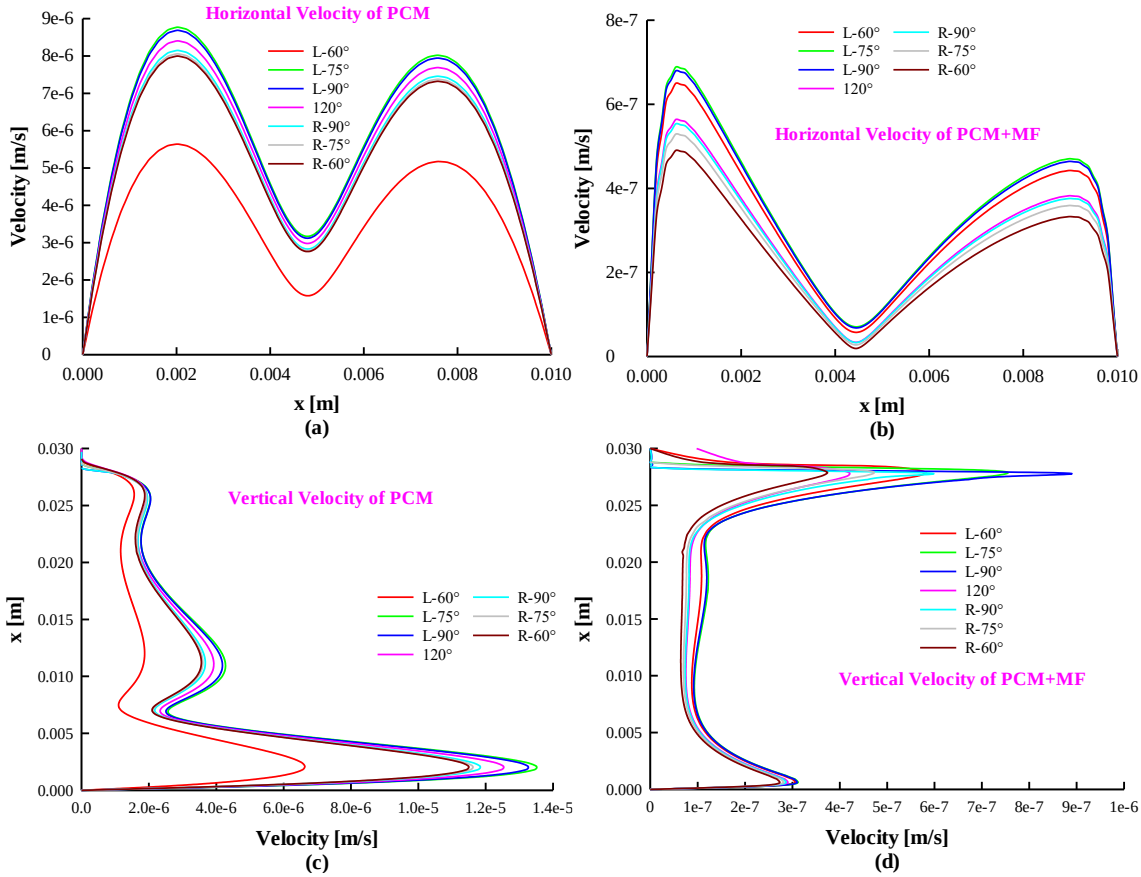

Figure 8. Velocity profile for; (a) without MF horizontal direction, (b) with MF horizontal direction, (c) without MF vertical direction, and (d) with MF vertical direction.

Demonstrating the results of ΔH changes in PCM applications provides a pioneering approach to determining energy storage capacity, design, and material selection. Figure 9 compares the ΔH performance of systems with and without MF over time for unit horizontal length. The results show that the ΔH trends are similar across both scenarios. Moreover, the energy storage process in systems with MF is more uniform, mirroring the homogeneity observed in liquid fraction and average temperature distributions. When the results are examined, it is calculated that the highest amount of stored energy is partially realized for the MF and without MF states of R-60°. In addition, when the without MF state and the MF state are compared for the full melting state, it is determined that the without MF state stores 5.69% more energy. The factor that causes this situation is that there is an aluminum material in the volume that should be PCM in the MF state, and this factor reduces the amount of energy stored in the MF state.

Another important situation determined is that the state containing MF stores higher energy from the beginning of the melting until the average temperature of the PCM reaches T_L=332K. At this point, the important issue and the decision which is within the user/system requirements is whether the full melting time or the total amount of stored energy is important. It is recommended that researchers optimize the porosity structures of the MFs to be used in LHTESs regarding this issue.

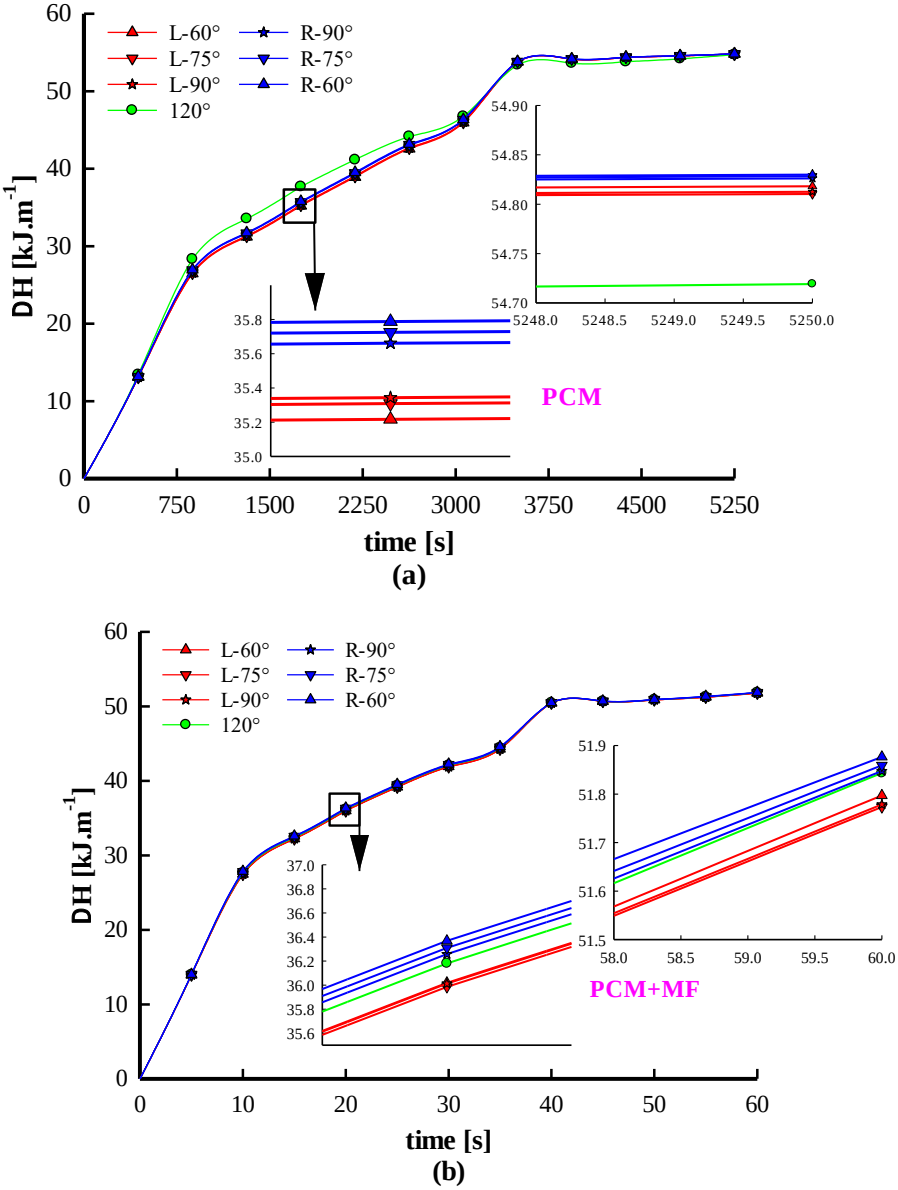

Figure 9. Energy storage versus time considering different IAs for; (a) without MF and (b) with MF.

IV. CONCLUSION

This study evaluates the performance of LHTES systems by investigating the effects of different IA triangular fins and MF. Key parameters such as liquid fraction, melting time, average temperature, and energy storage have been analyzed. The systems incorporate RT58 (Rubitherm) as PCM and aluminum MF with ε=0.9 and ω=20 PPI. In all simulations, the Brinkman-Darcy-Forchheimer model and enthalpy-porosity method were employed to solve the governing equations and model the melting process under the LTE hypothesis. The main findings are summarized as follows:

- *Reduction in Melting Time:* MF reduced the melting time by approximately 87.5 times due to the enhanced effective thermal conductivity, allowing heat to be conducted more efficiently within the cavity and increasing thermal diffusion.
- *Homogeneity of Liquid Fraction:* The PCM embedded within MF displayed a more uniform liquid fraction compared to the PCM without MF.

- *Melting Time Trends:* The shortest melting time occurred at 120° for systems without MF, while cases with MF experienced the earliest melting at R-60°, driven by the combined effects of enhanced heat conduction and convection.
- *Energy Storage:* Systems without MF exhibited higher energy storage than those with MF at the rate of 5.69% for R-60° since the volume occupied by the MF material is filled by the PCM which can store energy. The maximum amount of the stored energy is realized as 54.83 kJ.m-1.
- *Homogeneous Energy Storage:* Similar to the trends in liquid fraction and average temperature, the energy storage process in MF cases was more uniform, with the highest energy storage recorded as 51.87 kJ.m-1 at R-60°.
- *Possible studies:* In the next studies, the effects of different fin structures, the effects of different MF characteristics, the effects of nanoparticle use, the effects of magnetic field application and ultrasonic vibration application, and the cases including the combination of these applications can be addressed. Studies on the melting process and energy storage performance of LHTES can be conducted and also the solidification process of the system can be investigated.

CONFLICTS OF INTEREST

They reported that there was no conflict of interest between the authors and their respective institutions.

RESEARCH AND PUBLICATION ETHICS

In the studies carried out within the scope of this article, the rules of research and publication ethics were followed.

REFERENCES

[1] S. Tan and X. Zhang, "Progress of research on phase change energy storage materials in their thermal conductivity," *J. Energy Storage*, vol. 61, p. 106772, 2023, doi: https://doi.org/10.1016/j.est.2023.106772.

[2] B. K. Choure, T. Alam, and R. Kumar, "A review on heat transfer enhancement techniques for PCM based thermal energy storage system," *J. Energy Storage*, vol. 72, p. 108161, Nov. 2023, doi: 10.1016/J.EST.2023.108161.

[3] G. Liu *et al.*, "Experimental and numerical studies on melting/solidification of PCM in a horizontal tank filled with graded metal foam," *Sol. Energy Mater. Sol. Cells*, vol. 250, p. 112092, 2023, doi: https://doi.org/10.1016/j.solmat.2022.112092.

[4] S. Liu, H. Wang, Q. Ying, and L. Guo, "Numerical study on the combined application of multiple phase change materials and gradient metal foam in thermal energy storage device," *Appl. Therm. Eng.*, vol. 257, p. 124267, 2024, doi: https://doi.org/10.1016/j.applthermaleng.2024.124267.

[5] M. Xing, Z. Zhang, D. Jing, and H. Chen, "Enhanced solidification/melting heat transfer process by multiple copper metal foam for ice thermal energy storage," *J. Energy Storage*, vol. 79, p. 110207, 2024, doi: https://doi.org/10.1016/j.est.2023.110207.

[6] C. Yang *et al.*, "Analysis of charging performance of thermal energy storage system with graded metal foam structure and active flip method," *J. Energy Storage*, vol. 99, p. 113254, 2024, doi: https://doi.org/10.1016/j.est.2024.113254.

[7] S. Shen, H. Zhou, Y. Du, Y. Huo, and Z. Rao, "Investigation on latent heat energy storage using phase change material enhanced by gradient-porosity metal foam," *Appl. Therm. Eng.*, vol. 236, p. 121760, 2024, doi: https://doi.org/10.1016/j.applthermaleng.2023.121760.

[8] A. Alasmari *et al.*, "A shell-tube latent heat thermal energy storage: Influence of metal foam inserts in both shell and tube sides," *Int. Commun. Heat Mass Transf.*, vol. 159, p. 107992, 2024, doi: https://doi.org/10.1016/j.icheatmasstransfer.2024.107992.

[9] M. Bouzidi, M. Sheremet, K. Shank, S. Tiari, and M. Ghalambaz, "Charging and discharging heat transfer improvement of shell-tube storage utilizing a partial layer of anisotropic metal foam," *J. Energy Storage*, vol. 79, p. 109948, 2024, doi: https://doi.org/10.1016/j.est.2023.109948.

[10] W. Ahmed, A. Hussain, H. Shahid, I. Ali, and H. M. Ali, "Experimental Study on Heat Storage Properties Comparison of Paraffin/Metal Foams Phase Change Material Composites," *J. Therm. Sci.*, vol. 33, no. 2, pp. 469–478, 2024, doi: 10.1007/s11630-023-1828-5.

[11] A. Nassar *et al.*, "Enhancing the thermal transfer properties of phase change material for thermal energy storage by impregnating hybrid nanoparticles within copper foams," *Results Eng.*, vol. 21, p. 101885, 2024, doi: https://doi.org/10.1016/j.rineng.2024.101885.

[12] J. Liu, Y. Xiao, and C. Nie, "Pore-scale study of melting characteristic of phase change material embedded with novel open-celled metal foam," *Int. J. Heat Mass Transf.*, vol. 228, p. 125634, 2024, doi:

https://doi.org/10.1016/j.ijheatmasstransfer.2024.125634.
[13] Z. Du, X. Huang, Y. Li, X. Yang, and M.-J. Li, "Design and study of metal foam parameters on whole melting-solidification cycle in phase change heat storage system," *Int. J. Heat Fluid Flow*, vol. 106, p. 109299, 2024, doi: https://doi.org/10.1016/j.ijheatfluidflow.2024.109299.
[14] A. Moaveni, M. Siavashi, and S. Mousavi, "Passive and hybrid battery thermal management system by cooling flow control, employing nano-PCM, fins, and metal foam," *Energy*, vol. 288, p. 129809, 2024, doi: https://doi.org/10.1016/j.energy.2023.129809.
[15] C. Yang *et al.*, "Melting performance analysis of finned metal foam thermal energy storage tube under steady rotation," *Int. J. Heat Mass Transf.*, vol. 226, p. 125458, 2024, doi: https://doi.org/10.1016/j.ijheatmasstransfer.2024.125458.
[16] Y. Lu *et al.*, "Melting enhancement in a shell-and-tube latent heat storage unit with staggered fin-foam synergistic configuration," *J. Energy Storage*, vol. 82, p. 110505, 2024, doi: https://doi.org/10.1016/j.est.2024.110505.
[17] S. Rahmanian, Rahmanian-Koushkaki, M. H., Moein-Jahromi, and M. Setareh, "Numerical thermal performance assessment of phase change process in a PCM/foam-fins enclosure under various thermal conditions," *Energy Sources, Part A Recover. Util. Environ. Eff.*, vol. 46, pp. 2360–2376, 2024, doi: https://doi.org/10.1080/15567036.2024.2304642.
[18] P. M. Z. Hasan, N. H. Abu-Hamdeh, O. K. Nusier, A. M. Hussin, and H. A. Saad, "Energy storage analysis during melting in presence of metallic fins via numerical method," *J. Energy Storage*, vol. 66, p. 107454, 2023, doi: https://doi.org/10.1016/j.est.2023.107454.
[19] S. Zhang, L. Pu, L. Xu, and M. Dai, "Study on dominant heat transfer mechanism in vertical smooth/finned-tube thermal energy storage during charging process," *Appl. Therm. Eng.*, vol. 204, p. 117935, 2022, doi: https://doi.org/10.1016/j.applthermaleng.2021.117935.
[20] A. S, A. Sharma, and H. B. Kothadia, "Performance analysis of PCM melting in a fin-assisted thermal energy storage system – A numerical study," *Int. Commun. Heat Mass Transf.*, vol. 144, p. 106747, 2023, doi: https://doi.org/10.1016/j.icheatmasstransfer.2023.106747.
[21] M. K. Fahad, N. F. Ifraj, M. R. Haque, N. M. Chowdhury, and Fatema-Tuj-Zohora, "Numerical investigation on consecutive charging and discharging of PCM with Modified longitudinal fins in shell and tube thermal energy storage," *Results Eng.*, vol. 24, p. 103577, 2024, doi: https://doi.org/10.1016/j.rineng.2024.103577.
[22] S. D. Farahani, A. D. Farahani, A. J. Mamoei, and W.-M. Yan, "Enhancement of phase change material melting using nanoparticles and magnetic field in the thermal energy storage system with strip fins," *J. Energy Storage*, vol. 57, p. 106282, 2023, doi: https://doi.org/10.1016/j.est.2022.106282.
[23] C. Ao, S. Yan, L. Zhao, and Y. Wu, "Assessment on the effect of longitudinal fins upon melting process in a latent heat thermal energy storage unit," *J. Energy Storage*, vol. 59, p. 106408, 2023, doi: https://doi.org/10.1016/j.est.2022.106408.
[24] Z. Du, X. Huang, Y. Li, G. Liu, X. Yang, and B. Sundén, "Experimental Study on Melting and Solidification Cycle of a Hybrid Pin Fin/Metal Foam Energy Storage Tank," *ASME J. Heat Mass Transf.*, vol. 146, no. 8, p. 82401, 2024, doi: 10.1115/1.4065349.
[25] X. Huang, Z. Du, Y. Li, X. Yang, and M.-J. Li, "Numerical and optimization study on heat storage and release process of novel fin-metal foam composite structures under periodic heat source," *Int. J. Heat Fluid Flow*, vol. 108, p. 109445, 2024, doi: https://doi.org/10.1016/j.ijheatfluidflow.2024.109445.
[26] K. Zeng *et al.*, "Comprehensive enhancement of melting-solidifying process in latent heat storage based on eccentric fin-foam combination," *Energy*, vol. 313, p. 133693, 2024, doi: https://doi.org/10.1016/j.energy.2024.133693.
[27] A. NematpourKeshteli, M. Iasiello, G. Langella, and N. Bianco, "Increasing melting and solidification performances of a phase change material-based flat plate solar collector equipped with metal foams, nanoparticles, and wavy wall-Y-shaped surface," *Energy Convers. Manag.*, vol. 291, p. 117268, 2023, doi: https://doi.org/10.1016/j.enconman.2023.117268.
[28] I. Afaynou, H. Faraji, K. Choukairy, A. Arshad, and M. Arıcı, "Heat transfer enhancement of phase-change materials (PCMs) based thermal management systems for electronic components: A review of recent advances," *Int. Commun. Heat Mass Transf.*, vol. 143, p. 106690, Apr. 2023, doi: 10.1016/J.ICHEATMASSTRANSFER.2023.106690.
[29] T. Chen *et al.*, "Investigation and optimal design of partially encapsulated metal foam in a latent heat storage unit for buildings," *J. Energy Storage*, vol. 84, p. 110979, 2024, doi: https://doi.org/10.1016/j.est.2024.110979.
[30] B. Buonomo, H. Celik, D. Ercole, O. Manca, and M. Mobedi, "Numerical study on latent thermal energy storage systems with aluminum foam in local thermal equilibrium," *Appl. Therm. Eng.*, vol. 159, p. 113980, 2019, doi: https://doi.org/10.1016/j.applthermaleng.2019.113980.
[31] W. Lin, G. Xie, J. Yuan, and B. Sundén, "Comparison and Analysis of Heat Transfer in Aluminum Foam Using Local Thermal Equilibrium or Nonequilibrium Model," *Heat Transf. Eng.*, vol. 37, no. 3–4, pp. 314–322, Mar. 2016, doi: 10.1080/01457632.2015.1052682.
[32] A. D. Canonsburg, "ANSYS Fluent User ' s Guide," no. August. ANSYS, Inc., 2018.
[33] B. Buonomo, M. R. Golia, O. Manca, S. Nardini, and R. E. Plomitallo, "External heat losses effect on shell and tube latent heat thermal energy storages partially filled with metal foam," *J. Energy Storage*, vol. 85, p. 111096, Apr. 2024,

doi: 10.1016/J.EST.2024.111096.
[34] C. Nie, J. Liu, and S. Deng, "Effect of geometry modification on the thermal response of composite metal foam/phase change material for thermal energy storage," *Int. J. Heat Mass Transf.*, vol. 165, p. 120652, Feb. 2021, doi: 10.1016/J.IJHEATMASSTRANSFER.2020.120652.
[35] S. Huang, J. Lu, and Y. Li, "Numerical study on the influence of inclination angle on the melting behaviour of metal foam-PCM latent heat storage units," *Energy*, vol. 239, p. 122489, Jan. 2022, doi: 10.1016/J.ENERGY.2021.122489.
[36] F. Oflaz, "Evaluation of the thermo-hydraulic behavior of water-based graphene and Al2O3 hybrid nanofluids in a circular tube through CFD simulations," *J. Therm. Anal. Calorim.*, 2025, doi: 10.1007/s10973-025-13993-4.
[37] M. H. Zolfagharnasab, M. Salimi, and C. Aghanajafi, "Application of non-pressure-based coupled procedures for the solution of heat and mass transfer for the incompressible fluid flow phenomenon," *Int. J. Heat Mass Transf.*, vol. 181, p. 121851, 2021, doi: https://doi.org/10.1016/j.ijheatmasstransfer.2021.121851.
[38] T. Saeed, "Influence of the number of holes and two types of PCM in brick on the heat flux passing through the wall of a building on a sunny day in Medina, Saudi Arabia," *J. Build. Eng.*, vol. 50, p. 104215, 2022, doi: https://doi.org/10.1016/j.jobe.2022.104215.
[39] S. Patankar, *Numerical heat transfer and fluid flow*. CRC press, 2018.
[40] H. K. Versteeg, *An introduction to computational fluid dynamics the finite volume method, 2/E*. Pearson Education India, 2007.
[41] C. Z. Ji, Z. Qin, Z. H. Low, S. Dubey, F. H. Choo, and F. Duan, "Transient numerical study on enhancement of phase change material thermal storage with angled parallel fins," 2017.
[42] Ansys Inc., "Ansys Fluent User Guide," 2019. https://www.afs.enea.it/project/neptunius/docs/fluent/html/th/node352.htm